Vitamin B6 resensitizes *mcr*-carrying Gram-negative bacteria to colistin

Check for updates

Tianqi Xu[1], Dan Fang[1], Fulei Li[1], Zhiqiang Wang [1,2] ✉ & Yuan Liu [1,2,3] ✉

Antimicrobial resistance poses a severe threat to human health, with colistin serving as a critical medication in clinical trials against multidrug-resistant Gram-negative bacteria. However, the efficacy of colistin is increasingly compromised due to the rise of MCR-positive bacteria worldwide. Here, we reveal a notable metabolic disparity between *mcr*-positive and -negative bacteria through transcriptome and metabolomics analysis. Specifically, pyridoxal 5'-phosphate (PLP), the active form of vitamin B6, was significantly diminished in *mcr*-positive bacteria. Conversely, supplementing with PLP could reverse the metabolic profile of drug-resistant bacteria and effectively restore colistin's bactericidal properties. Mechanistically, PLP was found to augment bacterial proton motive force by inhibiting the Kdp transport system, a bacterial K^+ transport ATPase, thereby facilitating the binding of the positively charged colistin to the negatively charged bacterial membrane components. Furthermore, PLP supplementation triggers ferroptosis-like death by accumulating ferrous ions and inducing lipid peroxidation. These two modes of action collectively resensitize *mcr*-harboring Gram-negative bacteria to colistin therapy. Altogether, our study provides a novel metabolic-driven antibiotic sensitization strategy to tackle antibiotic resistance and identifies a potentially safe antibiotic synergist.

Colistin, also known as polymyxin E, is a bactericidal antibiotic effective against a wide range of Gram-negative bacteria[1]. Colistin was discovered in the late 1940s, but due to its toxicity, mainly nephrotoxicity, it was withdrawn from the first line[2]. However, the emergence of multidrug-resistant (MDR) bacteria, especially *Acinetobacter baumannii*, *Pseudomonas aeruginosa*, and *Klebsiella pneumoniae*, constitutes a major threat to global health[3]. The scarcity of new antibiotics has led to a renewed interest in colistin as a last resort for combating MDR bacteria. Unfortunately, bacteria have developed multiple resistance mechanisms to withstand colistin therapy, among which the plasmid-mediated colistin resistance gene *mcr* has posed a significant challenge[4]. The *mcr* gene encodes phosphoethanolamine transferase, which modifies lipopolysaccharide (LPS), thereby reducing the binding affinity of LPS to colistin[5,6]. This underscores the urgency of developing innovative strategies to tackle *mcr*-mediated mobile colistin resistance.

Accumulating evidence highlights a close relationship between the metabolic state of bacteria and their susceptibility to antibiotics[7]. Prior research has demonstrated that antibiotic or disinfectant pressure can inhibit bacterial metabolism, characterized by reduced aerobic respiration, ATP generation suppression, and proton motive force dissipation, thereby enhancing bacterial tolerance to antibiotics[8–10]. Furthermore, there is an intricate connection between bacterial metabolism and antibiotic resistance. Alterations in the tricarboxylic acid (TCA) cycle, aerobic respiratory chain, and metal ion metabolisms, such as iron, can influence bacterial sensitivity to antibiotics[11]. For instance, *Escherichia coli* strains lacking isocitrate dehydrogenase (*IDH*)[12] or aconitase B (*acnB*)[13] exhibit resistance to quinolones. Mutations in cytochrome genes (*cycB*) and genes involved in NADH reduction (*nuo* and *nqr*) confer resistance to tobramycin in *P. aeruginosa*[14]. Additionally, an imbalance in intracellular iron homeostasis in bacteria also impacts the effectiveness of antibiotics. It has been shown that iron can augment the resistance of *Actinomycetes* to bactericidal antibiotics by promoting respiration[15], and the deletion of ferredoxin-NADP reductase (*FprB*) confers increased antibacterial drug resistance to *Pseudomonas* species[16].

The acquisition of resistance also imposes a metabolic burden on bacteria[11]. Accordingly, the overexpression of the colistin resistance gene *mcr-1* induces metabolic disorders in the pentose phosphate pathway[17]. Therefore, modulating bacterial metabolism provides a feasible strategy to

[1]Jiangsu Co-innovation Center for Prevention and Control of Important Animal Infectious Diseases and Zoonoses, College of Veterinary Medicine, Yangzhou University, Yangzhou, China. [2]Joint International Research Laboratory of Agriculture and Agri-Product Safety, the Ministry of Education of China, Yangzhou University, Yangzhou, China. [3]Institute of Comparative Medicine, Yangzhou University, Yangzhou, China. ✉e-mail: zqwang@yzu.edu.cn; liuyuan2018@yzu.edu.cn

resensitize drug-resistant bacteria to antibiotics, an approach termed metabolic reprogramming. For example, a series of metabolites, including indole[9], thymine[18], glutamine[19], alanine and/or glucose[20] have been found to boost the bactericidal effect of antibiotics by reprogramming bacterial metabolism.

Pyridoxal 5′-phosphate (PLP), the biologically active form of vitamin B6, serves as a cofactor that catalyzes 238 different types of enzyme reactions[21,22]. It participates in various biological processes, including amino acid metabolism, sugar metabolism, and lipid metabolism. PLP is typically administered through tablets or injections, with the recommended daily intake for adults being 1.4 mg[23]. Studies have shown that there are over 140 PLP-dependent enzymes[24]. In prokaryotic organisms, ~1.5% of the genes are dedicated to encoding PLP-dependent enzymes[22]. Notably, plasma PLP levels has been found to be inversely correlated with the risk of cardiovascular disease[25], venous thrombosis[26], diabetes[27], and inflammatory bowel disease (IBD)[28]. PLP-dependent enzymes have also been explored as potential drug targets and antibiotic hits[29], highlighting their therapeutic potential in the treatment of various illnesses.

In this study, we investigated the metabolic differences between *mcr-1*-negative and -positive bacteria, and identified the critical metabolite PLP, which can reshape the metabolic flux of *mcr-1*-positive bacteria. Interestingly, we found that PLP enhanced colistin's lethal effect on drug-resistant Gram-negative bacteria both in vitro and in vivo, highlighting a novel metabolism-driven antibiotic sensitization therapy. PLP works by blocking the Kdp system and increasing bacterial proton motive force. Meanwhile, as a cofactor of protein Cys, PLP-induced lipid peroxidation causes ferroptosis-like death, which aids in killing *mcr*-positive bacteria in combination with colistin.

Results

mcr-1 expression alters bacterial transcriptional regulation and metabolism

To explore the metabolic difference between colistin-susceptible and -resistant *E. coli*, we amplified *mcr-1* gene along with its promoter and cloned them into the pUC19 plasmid, generating pUC19-*mcr-1*. Meanwhile, pUC19 was used as a control vector. Then, both plasmids were respectively transformed into *E. coli* DH5α, with DH5α (pUC19) representing the colistin-susceptible strain and DH5α (pUC19-*mcr-1*) representing the colistin-resistant strain. The minimum inhibitory concentration (MIC) of colistin in DH5α (pUC19) was 0.0625 μg/mL, while its MIC value in DH5α (pUC19-*mcr-1*) was elevated by 32-fold (2 μg/mL, Table S1), confirming the functional activity of the *mcr-1* plasmid and its role in conferring colistin resistance.

Then, we performed transcriptome analysis of *mcr*-negative and -positive bacteria. The results showed that there were significant differences in transcription between colistin-susceptible and -resistant bacteria. Excluding shared genes, there was a series of differentially expressed genes (DEGs, fold change ≥ 2-fold) in two groups. Comparing the pUC19 and pUC19-*mcr-1* groups, 295 DEGs were up-regulated and 315 DEGs were down-regulated in the pUC19 group. While in the pUC19-*mcr-1* group, 178 genes were up-regulated, and 147 genes were down-regulated (Fig. S1a). Kyoto Encyclopedia of Genes and Genomes (KEGG) enrichment analysis showed that these up-regulated DEGs were mainly related to lipopolysaccharide (LPS) biosynthesis, which may be due to the modifications in LPS mediated by *mcr-1*, while these downregulated DEGs were involved in TCA cycle (Fig. S1c). Consistently, Gene Ontology (GO) enrichment is mainly involved in lipopolysaccharide core region metabolic and some metabolic processes, including biosynthetic process, respiratory chain complex and fatty acid catabolic process (Fig. S1d).

It has been shown that the metabolic state influences bacterial susceptibility to antibiotics[7]. Under the same culture medium without colistin, DH5α (pUC19) and DH5α (pUC19-*mcr-1*) were analyzed by untargeted metabolomics to determine their metabolic characteristics. Through principal component analysis (PCA), the two strains could be clearly separated from each other (Fig. 1b). The metabolites that exhibited significant differences between the two bacterial strains were identified using OPLS-DA analysis (VIP > 1, *P* < 0.05, Fig. 1c). A total of 64 known metabolites were significantly changed, among which there were 36 up-regulated metabolites and 28 down-regulated comparing the pUC19 and pUC19-*mcr-1* groups. Among these, after removing metabolites without KEGG pathway ID, 33 representative metabolites were screened based on metabolic pathways (Fig. 1d). *Z*-score showing changes in metabolites with 20 metabolites at the lower abundance and 13 metabolites at the higher abundance (Fig. 1e). These metabolites were classified as amino acids and amines; cofactors, nucleotides and bases; neurotransmitters and monosaccharides (Fig. 1f). Meanwhile, KEGG enrichment analysis showed that differential metabolites were partly involved in oxidative phosphorylation and protein digestion and absorption (Fig. 1g). To intuitively study the differences in transcription and metabolism between colistin-sensitive and -resistant bacteria, we also used iPath3.0 to visualize transcription and metabolic pathways. The results indicated that these differential pathways were predominantly enriched in the energy metabolism, amino acid metabolism, and lipid metabolism pathways (Fig. S1e). Taken together, these results indicate that *mcr* expression results in the shift of bacterial transcription and metabolism.

PLP reverses *mcr*-mediated colistin resistance in vitro

Out of these metabolites, after removing insoluble metabolites such as 2'-deoxyadenosine 5'-monophosphate, toxic metabolites such as phenylethylamine, and metabolites with antibacterial activity such as 3-(4-hydroxyphenyl)lactic acid, we screened 12 metabolites for follow-up experiments in combination with the KEGG pathway, toxicity and solubility. In the following bactericidal experiment, we evaluated the effect of metabolites on bactericidal activity of colistin (Fig. 2a). The results showed that pyridoxal 5'-phosphate (PLP), also known as the active form of vitamin B6, can effectively enhance the killing of colistin against *mcr-1*-positive *E. coli* G92 (Fig. 2b, Table S2). Consistently, an alternation in PLP-dependent enzymes was also observed from the transcriptome results (Fig. S1b). To further explore the potentiation of PLP to colistin, four *mcr*-positive bacteria were exposed to different concentrations of PLP. Interestingly, we found that PLP exhibited a potentiating effect on colistin in a dose-dependent manner, even for different species of bacteria, including *S. enterica* SC2016090 and *K. pneumoniae* D120 (Fig. 2c). Next, we used live/dead fluorescent staining probes to stain the bacteria. Flow cytometry results showed that PLP supplementation increased the death of *mcr*-positive bacteria compared with colistin alone (Fig. 2d), which was consistent with the results of laser confocal microscopy (Figs. 2e, S3a). Meanwhile, the bacterial growth curve results demonstrated that the combination of PLP and colistin limited bacterial proliferation. In contrast, PLP supplementation alone did not influence bacterial growth, indicating that PLP, by itself, did not impose a fitness burden on bacteria (Fig. 2f).

To investigate the impact of PLP on the evolution of colistin resistance, we serially passaged *E. coli* G92 in media containing colistin alone or in combination with PLP over a period of 20 days. The results showed an 8-fold increase in colistin MIC values in the presence of sub-MICs of colistin alone. In contrast, a 2-fold reduction in colistin MICs was observed in the combination group (Fig. 2g), indicating that PLP effectively inhibited the development of colistin resistance. Moreover, we performed whole-genome sequencing (WGS) and single nucleotide polymorphisms (SNPs) analysis on the passaged strains. The results identified 60 mutations in the colistin-alone group, compared to only 9 mutations in the combination group (Tables S3, S4). Notably, mutations in colistin resistance-associated genes, such as the two-component transcriptional regulatory proteins BasR/PmrA[30], were absent in the presence of PLP. Together, these results demonstrated that PLP effectively resensitizes *mcr*-carrying bacteria to colistin and thwarts the resistance evolution.

PLP enhances bacterial proton motive force by downregulating the KDP transporter

To dissect the underlying mechanisms by which PLP restores the susceptibility of drug-resistant bacteria to colistin, we performed transcriptome
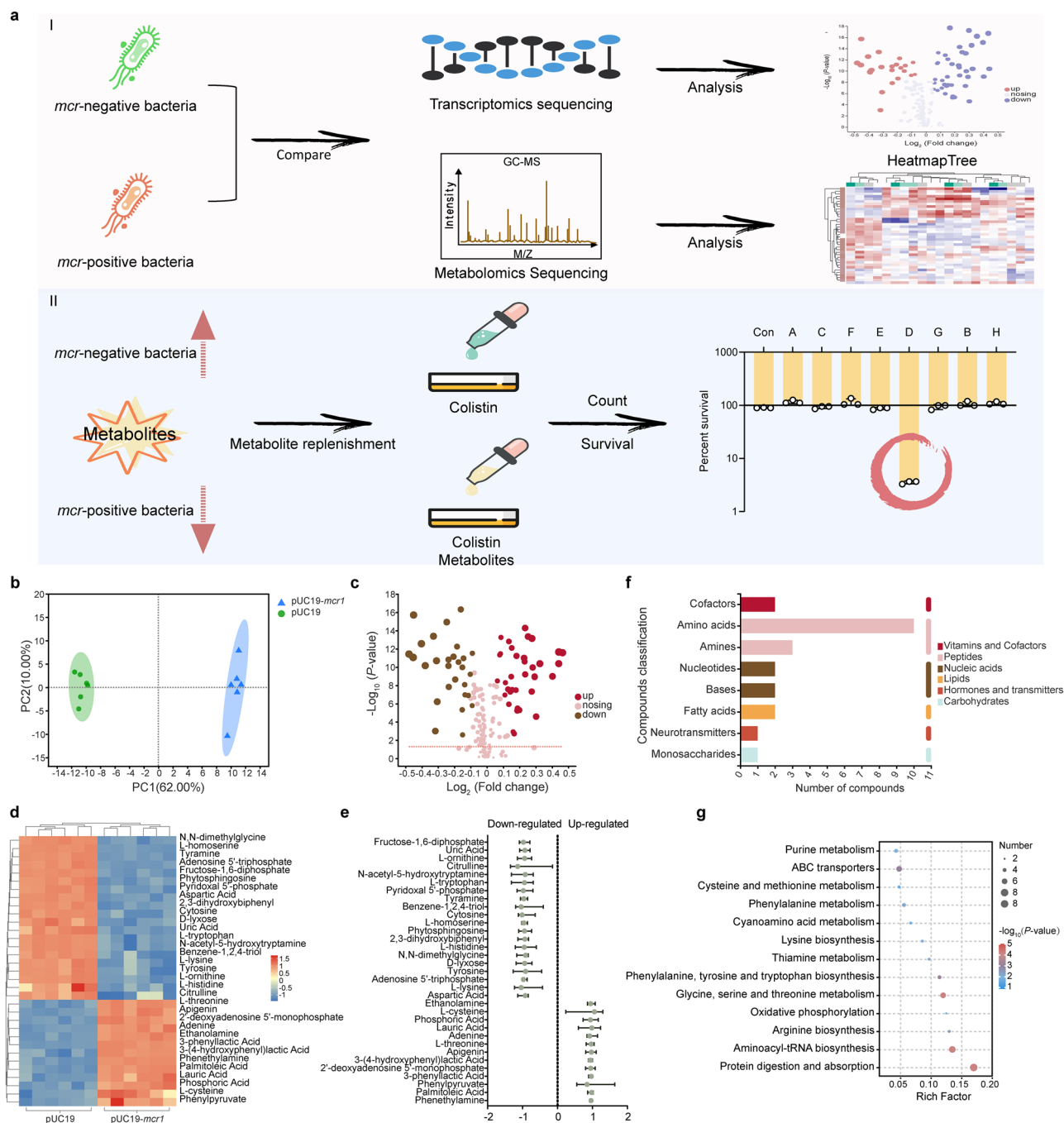
Fig. 1 | Differential metabolome analysis of *mcr*-negative and -positive bacteria. **a** Scheme of the experimental protocols. Part I: The differences in transcription and metabolism between *mcr*-negative and -positive bacteria through transcriptomics and metabolomics. Part II: Differential metabolites that were upregulated in *mcr*-negative bacteria but downregulated in *mcr*-positive bacteria when using colistin for bactericidal experiments. Then, metabolites that can decrease bacterial survival rates were screened. **b** PCA score plots of the first two components for metabolite levels from *E. coli* DH5α (pUC19) and *E. coli* DH5α (pUC19-*mcr-1*). $n = 6$ biologically independent replicates. **c** Volcano-plot of differential metabolites. Log$_2$-fold changes (Log$_2$(FC)) in metabolites in *E. coli* DH5α (pUC19) versus *E. coli* DH5α (pUC19-*mcr-1*) and the corresponding significance values displayed as log$_{10}$ (*P*-value). Red dots represent significantly upregulated metabolites, while brown dots represent significantly down-regulated metabolites. **d** Heat map for relative abundances of differential metabolites with KEGG pathway in *E. coli* DH5α (pUC19) compared with *E. coli* DH5α (pUC19-*mcr-1*). A column in the heat map represents an individual sample, and a row represents an individual metabolite. Color shades indicate changes in increased (orange) or decreased (blue) metabolite levels relative to the median metabolite level. **e** Z-score plot of metabolites of *E. coli* DH5α (pUC19) versus *E. coli* DH5α (pUC19-*mcr-1*), corresponding to data in (**d**). **f** The numbers of differential metabolites in six classifications. **g** The top 13 KEGG enrichment pathways of differential metabolites. Bubble size indicates the number of metabolites annotated to a KEGG Pathway. Color shades indicate the corresponding significance values as log$_{10}$ (*P*-value).

analysis of *E. coli* G92 in the absence or presence of PLP. Principal component analysis (PCA) was employed to identify notable distinctions between the groups with or without PLP treatment (Fig. S2a). Notably, the supplementation of PLP resulted in a total of 1311 differentially expressed genes (DEGs). Among these genes, 706 genes were found to be up-regulated, while 605 genes were down-regulated (Fig. S2b). Further analysis using KEGG enrichment demonstrated that these DEGs were primarily associated with sulfur metabolism and the two-component system (Figs. 3a,
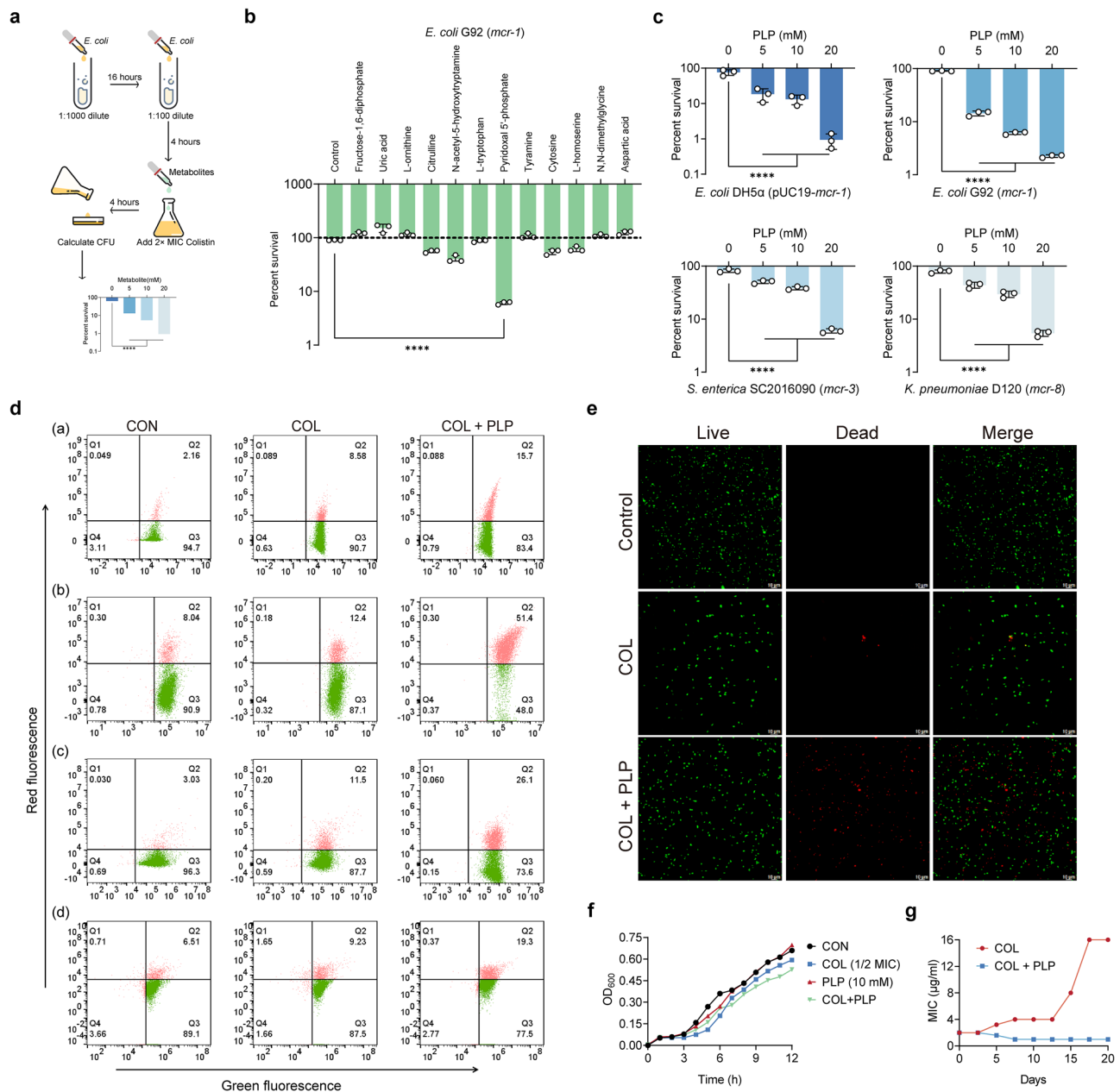
Fig. 2 | PLP enhances the effectiveness of colistin against *mcr*-carrying bacteria. **a** Scheme of the experimental protocols. The *mcr*-positive bacteria were present in the 1:1000 dilution and grown for 16 h. Then, the mixture was diluted 1:100 in 20 mL of fresh MHB medium. After culturing for 4 h, bacteria were resuspended in M9CA medium. Colistin (2-fold MIC) and chosen metabolites were added for another 4 h. Monitored relative survival through colony forming units (CFU) count. **b** Percent survival of *E. coli* G92 in the presence of chosen metabolites (10 mM) plus colistin (4 μg/mL) after co-culture. **c** Percent survival of different *mcr*-positive bacteria in the presence of increasing concentrations of PLP (0-20 mM) plus colistin (2-fold MIC). **d** The Live/Dead BacLight viability assay was performed by flow cytometry on *E. coli* DH5α (pUC19-*mcr-1* (**a**)), *E. coli* G92 (*mcr-1* (**b**)), *S.enterica* SC2016090 (*mcr-3* (**c**)) and *K. pneumoniae* D120 (*mcr-8* (**d**)) treated with colistin (2-fold MIC) or combined

with PLP (10 mM) for 4 h. SYTO 9 staining was used to demonstrate live cells, while propidium iodide staining was used to demonstrate dead cells. **e** Confocal scanning microscopy imaging of live and dead states of *E. coli* G92 when cultured with colistin alone (2-fold MIC) or in combination with PLP (10 mM) for 4 h. The left image was SYTO 9 staining (live cells), the middle image was PI staining (dead cells), and the right image was a merged image of live cells (green) and dead cells (red). **f** Curves comparing bacterial growth (OD_{600}) of *E. coli* G92 with or without PLP (10 mM) in the presence or absence of colistin (1 μg/mL). **g** MICs of *E. coli* G92 passaged for 40 generations in the presence or absence of PLP (20 mM). All data from three biological replicates were presented as mean ± SD, and statistical significance was determined by non-parametric one-way ANOVA. ***$P < 0.001$, ****$P < 0.0001$.

S2c). Consistently, GO enrichment analysis was mainly involved in metabolic and biological processes (Fig. S2d). To gain a more comprehensive understanding of the influence of PLP on bacterial metabolism, we employed iPath3.0 as a tool for visualizing the essential metabolic pathways (Fig. S2e).

Transcriptomic analysis revealed significant alterations in the transcription of genes related to the two-component system (*kdpFABC* and

kdpDE), both linked to the Kdp transporter[31]. We next validated the expression of these genes using RT-qPCR and found that the transcription of *kdpA*, *kdpC* and *kdpD* was significantly down-regulated (Fig. 3b), suggesting that the Kdp transport system was inhibited in *mcr*-positive bacteria after exposure to PLP. Given that the Kdp system is a high-affinity potassium transport system[32], we employed a fluorescent probe potassium-binding benzofuran isophthalate (PBFI) to assess K^+ transport activity,

Fig. 3 | PLP enhances the proton motive force by activating the Kdp system. a Selected differential expression genes (after Min–Max normalization) involved in sulfur metabolism, biosynthesis of siderophore group, two-component system, lipid oxidation, antioxidant and cysteine metabolism. **b** RT-qPCR analysis for the expression of *kdpA*, *kdpC* and *kdpD* of *E. coli* G92 in the absence or presence of PLP. **c** The fluorescence intensity ratio (340/380) represents the intracellular K$^+$ concentration in *E. coli* G92 after co-cultured with increasing concentrations of PLP (ranging from 0 to 20 mM), with the aid of a fluorescence dye PBFI-AM (5 μM). **d** Membrane potential changes induced by PLP (ranging from 0 to 20 mM), determined using a fluorescence dye DiSC$_3$(5) (5 μM). **e** The mean fluorescence intensity ratio (red/green) indicates the PMF of *E. coli* G92, incubated with DiOC$_2$(3) for 20 min in the presence of different concentrations of PLP (ranging from 0 to 20 mM). CCCP was used as a PMF inhibitor. **f** ATP content in *E. coli* G92 after co-cultured with increasing concentrations of PLP (ranging from 0 to 20 mM). **g** Percent survival of *E. coli* G92 in the presence of PLP (10 mM) and colistin (4 μg/mL) plus the indicated concentrations of CCCP (ranging from 0 to 10 mM). **h** The assimilation of colistin of *E. coli* G92 after cultured with colistin (0.5 μg/mL) and PLP (ranging from 0 to 20 mM). **i** Outer membrane integrity changes of *E. coli* G92 after co-cultured with PLP (ranging from 0 to 20 mM), determined using the fluorescence dye 1-*N*-phenylnaphthylamine (NPN, 10 μM). **j** Inner membrane integrity changes of *E. coli* G92 after co-cultured with colistin (ranging from 0 to 4 μg/mL) and PLP (10 mM), determined using the fluorescence dye propidium iodide (PI, 5 μM). **k** Schematic diagram of the underlying mechanisms by which PLP increases PMF by activating the Kdp system, thereby attenuating *E. coli* G92 resistance to colistin. All data from three biological replicates were presented as mean ± SD, and statistical significance was determined by non-parametric one-way ANOVA. *$P < 0.05$, **$P < 0.01$, ***$P < 0.001$, ****$P < 0.0001$.
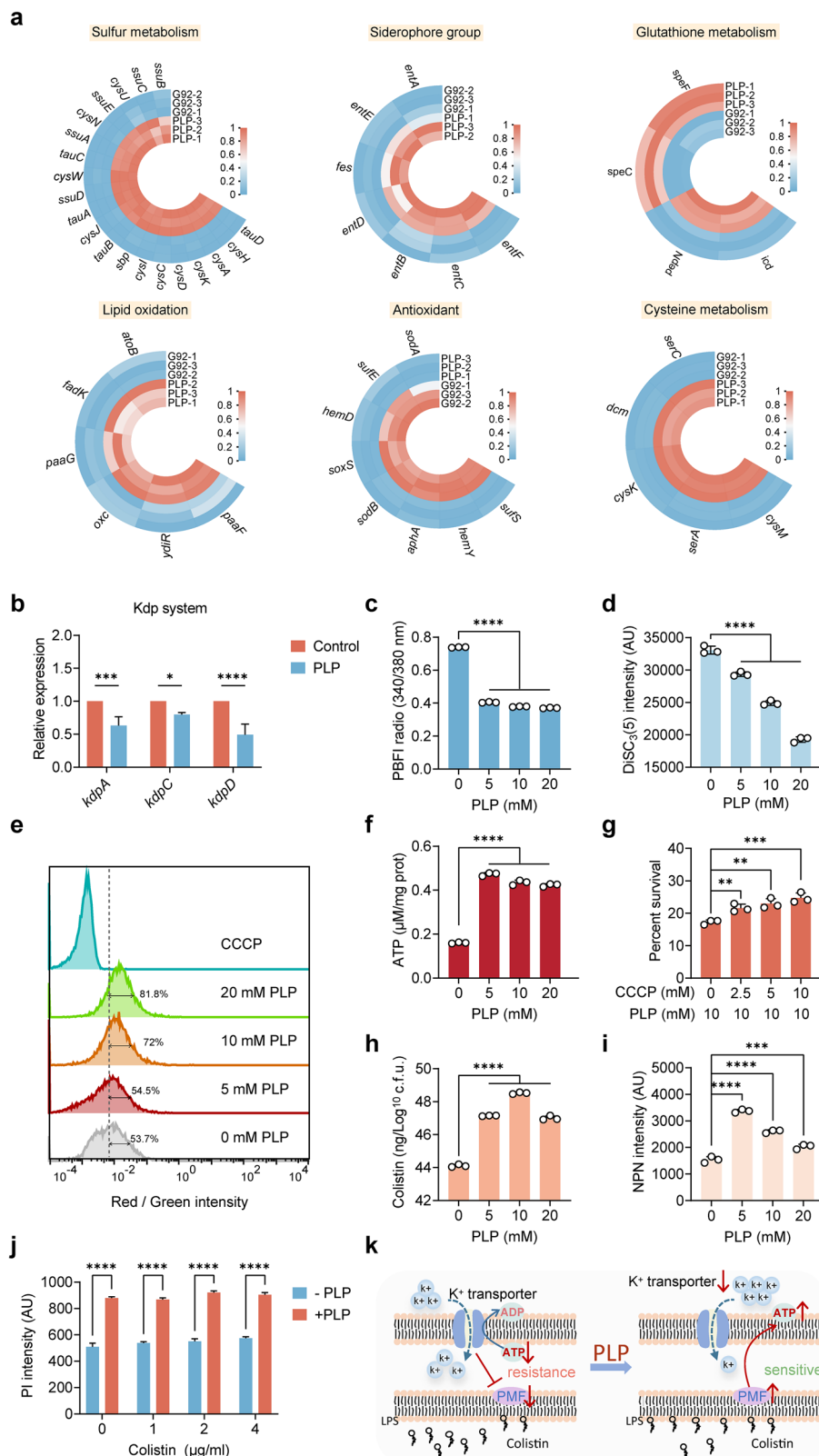
finding that PLP significantly impaired Kdp functionality (Fig. 3c). Inactivation of the Kdp system is known to hyperpolarize the transmembrane potential[32], so we measured membrane potential changes with the DiSC$_3$(5) probe, which showed that PLP markedly hyperpolarized the membrane (Fig. 3d). The transmembrane potential (ΔΨ) and proton gradient (ΔpH) contribute to the proton motive force (PMF), with the latter showing no

significant changes (Fig. S3b). Using DiOC$_2$(3) and flow cytometry, we quantified bacterial PMF under PLP, revealing that PLP significantly increased bacterial PMF (Figs. 3e, S3d). KdpFABC is an ATP-dependent enzyme[33], that is, the inactivation of Kdp system would lead to the accumulation of ATP. Consistently, an increase in intracellular ATP levels in bacteria exposed to PLP was observed (Fig. 3f).

A recent study showed that increased PMF promoted the binding between colistin and LPS[34]. We speculated that the increased PMF by the inactivated Kdp system may be responsible for the enhanced bactericidal effect of colistin. To verify it, carbonyl cyanide 3-chlorophenylhydrazone (CCCP), a known PMF inhibitor, was co-incubated with colistin and PLP, and we found that the addition of CCCP abolished the potentiation of PLP in a dose-dependent manner (Fig. 3g). Meanwhile, we found that PLP dramatically increased the accumulation of colistin within the cells (Fig. 3h). Considering that the bactericidal effect of colistin is mainly to destroy the bacterial cell membrane[35], we further examined changes in membrane integrity (Fig. 3i) and permeability (Fig. 3j) upon the addition of PLP. We found that PLP could enhance the permeability in a dose-dependent manner, accompanied by disruption of membrane integrity, indicating disruption of both the inner and outer membranes. These points indicated that PLP could enhance the destruction of colistin on the membrane of *mcr*-positive bacteria. All the above experimental results support the conclusion that PLP enhances PMF by specifically inhibiting the Kdp transporter, which in turn increases the affinity between colistin and LPS, as well as the colistin action on membrane permeability (Fig. 3k).

PLP impairs bacterial defense system and aggravates oxidative damage

The transcriptome analysis showed that sulfur metabolism was significantly enhanced upon PLP treatment (Figs. 3a and 4a). Of those, the transcript level of the *cysK* gene encoding cysteine synthase A, a pyridoxal phosphate-dependent enzyme[36], was significantly up-regulated by PLP. Meanwhile, the transcription levels of genes related to cysteine metabolism and glutathione metabolism were significantly changed (Fig. 3a). Given that the loss of cysK results in the accumulation of H$_2$S and a substantial reduction in cysteine content[37], we monitored the changes of H$_2$S and cysteine upon PLP addition. Using lead acetate paper strips, we found that PLP dose-dependently reduced the production of H$_2$S despite the presence of colistin (Fig. 4b). Meanwhile, the upregulation of CysK-mediated cysteine synthesis[38] promoted cysteine accumulation (Fig. 4c). Meanwhile, cysteine was easily oxidized by molecular oxygen into cystine[39], which exhibited a significant upregulation intracellularly (Fig. 4d). This observation was also evidenced by a decreased ratio of NAD$^+$ to NADH since the oxidation of cysteine can cause a redox imbalance (Fig. S3b).

H$_2$S is a universal defense that can protect bacteria against antibiotic-mediated reactive oxygen species (ROS) damage[40]. Additionally, given that antioxidant-related genes were markedly downregulated while genes associated with lipid oxidation were significantly up-regulated (Fig. 3a), we measured the production of intracellular ROS in the presence of PLP. The results presented that PLP augmented ROS production in a dose-dependent manner (Fig. 4e). Thiourea, a ROS scavenger[41], dramatically diminished the bactericidal efficacy of colistin in the presence of PLP after 8 h (Fig. 4f), highlighting the critical role of ROS in PLP-induced antibiotic potentiation.

Accumulating evidence suggests that superoxide dismutase (SOD) could oxidize H$_2$S and maintain intracellular ROS homeostasis[42]. Thus, we determined the activity of the SOD enzyme and oxidative damage-related genes (*sodA*, *sodB*, *oxyR*, *dps*) expression. The results showed that PLP reduced the expression of SOD-related genes (Fig. S4a) and inhibited its activity (Fig. 4g). In parallel, we also assessed SOS response genes, which are frequently induced by bactericidal antibiotics via hydroxyl radicals[43]. We found that SOS response-associated genes (*recA*, *recB*, *recD*, *umuD*, *dinD*) were downregulated, while the expression of *lexA*, a negative SOS regulator, was up-regulated (Fig. S4b), implicating that PLP inhibited the repair of oxidative damage. Taken together, the above results may indicate that PLP increases bacterial susceptibility to antibiotics by altering cellular redox potential and enhancing oxidative damage.

PLP induces bacterial ferroptosis-like death

Cysteine, a key component of glutathione (GSH) and a crucial antioxidant, rapidly oxidizes to cystine, which is essential for GSH synthesis. This oxidation process is coupled with the reduction of ferric iron (Fe^{3+}) to ferrous iron (Fe^{2+})[44]. Meanwhile, excessive cysteine consumption accelerates GSH depletion and enhances ROS production, leading to increased oxidative damage. To understand how PLP exacerbates this damage, we investigated intracellular ferrous ion concentrations and found that PLP treatment induced a dose-dependent increase in Fe^{2+} levels (Fig. 5a). Considering the link between ion homeostasis disruption and colistin activity[45], we postulated that PLP might induce ferroptosis, a form of cell death characterized by iron accumulation and driven by lipid peroxidation[46]. In agreement with our hypothesis, we found that PLP triggered the accumulation of toxic lipid peroxides (LPO) and malondialdehyde (MDA), indicative of enhanced oxidative stress (Fig. 5b and c). Using C11-BODIPY[581/591], an LPO sensor incorporated into the lipid membrane, we monitored cellular lipid peroxidation levels via flow cytometry[47]. The results showed that PLP potently induced bacterial lipid peroxidation in a dose-dependent manner (Fig. 5e). Consistent with these observations, similar effects were observed in *K. pneumoniae* D120 (*mcr-8*) (Fig. S5a) and *S. enterica* SC2016090 (*mcr-3*) (Fig. S5b), indicating that PLP-mediated lipid peroxidation is a general phenomenon and not limited to *E. coli*.

The accumulation of LPO and the depletion of GSH are the key factors of ferroptosis[48]. Cysteine can theoretically promote the synthesis of GSH, but under oxidative stress conditions, excess cysteine will be oxidized to cystine and accelerate the consumption of GSH by increasing the generation of ROS. Therefore, we assessed the balance of intracellular glutathione, and found a marked decrease in the ratio of reduced GSH to oxidized glutathione (GSSG), suggesting a disruption of glutathione homeostasis and the utilization of GSH to counteract oxidative stress (Fig. 5d). Of note, in the *mcr*-negative strain, GSH levels declined post-PLP treatment, yet GSSG levels remained unremarkably elevated (Fig. S4c). This disparity indicated that PLP had a lesser effect on *mcr*-negative bacteria compared to *mcr*-positive bacteria (Fig. S4d), implying that PLP induces oxidative stress more effectively in *mcr*-positive strains, potentially due to plasmid-mediated heightened susceptibility to oxidative damage. Scanning electron microscopy (SEM) analyses revealed that bacteria exposed to both colistin and PLP displayed hallmarks of ferroptosis-like cell death, such as cell membrane dissolution and cytoplasmic disintegration[49] (Fig. 5f). These findings underscore that PLP escalated Fe^{2+} accumulation and fostered lipid peroxidation.

To further verify these results, the metal ion chelator ethylenediaminetetraacetic acid (EDTA) was added into PLP for co-incubation with bacteria. The results showed that EDTA significantly hindered bacterial killing (Fig. S6a), suggesting that iron chelation could negate the potentiating effect of PLP. Similarly, other iron-binding agents, such as deferoxamine (DFO), also mitigated the action of PLP (Fig. S6b). Intriguingly, ferrostatin-1 (Fer-1), a known inhibitor of ferroptosis[50], substantially counteracted the enhancement of PLP on colistin (Fig. S6c). Subsequent experiments involving the co-incubation of bacteria with colistin and FINO2, a potent ferroptosis inducer[51], revealed that this inducer dose-dependently augmented the bactericidal efficacy of colistin (Figs. 5g and S7). The above results illustrate that PLP enhances the bactericidal activity of colistin by inducing bacterial ferroptosis-like death (Fig. 5h).

PLP rescues colistin effectiveness in vivo

Having demonstrated that PLP enhanced the bactericidal effect of colistin in vitro, we next investigated whether PLP could restore the efficacy of colistin in vivo. To assess this, we employed the *Galleria mellonella* infection models (Fig. 6a). Insect larvae were infected with *E. coli* G92 and then treated with a single dose of colistin with or without PLP. Consequently, we found that colistin and PLP combined treatment resulted in higher larvae survival compared with colistin monotreatment ($P = 0.0012$, Fig. 6c). Additionally, a mouse peritonitis sepsis model was applied to test the in vivo efficacy of combination therapy (Fig. 6b). Before infection, mice were orally administered PBS or PLP for five consecutive days. All mice were then infected
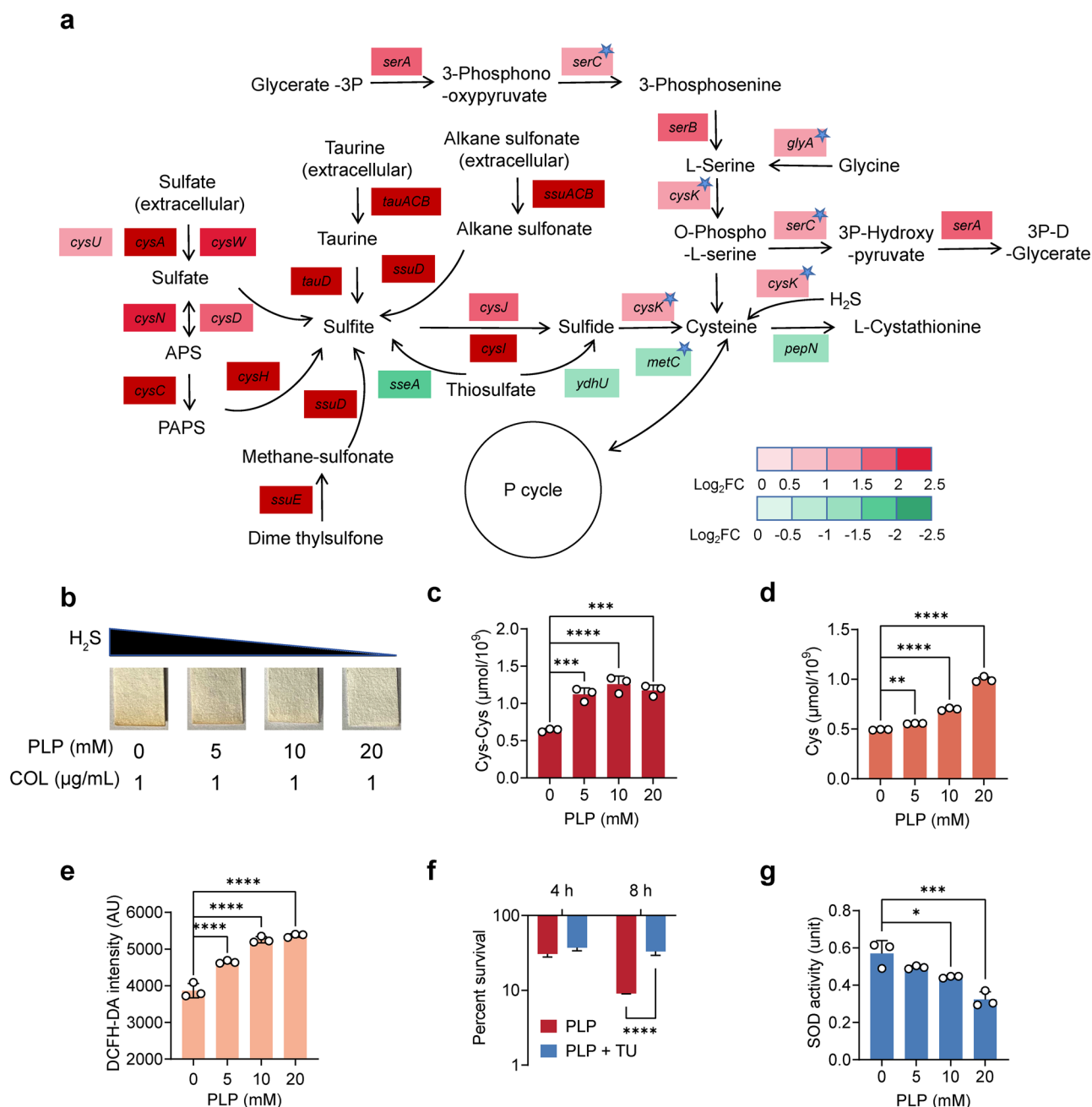
Fig. 4 | PLP induces oxidative damage by enhancing sulfur metabolism. a Selected differential expression genes involved in sulfur metabolism. Color shades indicate Log_2-fold changes of increased (red) or decreased (green) gene expression under exposure of PLP. The star symbol indicates that PLP is required as a coenzyme. **b** Semiquantitative calculation of H_2S produced by *E. coli* G92 after incubation with PLP (ranging from 0 to 20 mM) and colistin (1 μg/mL). As a result of the reaction between H_2S released by bacterial cultures and Pb $(Ac)_2$, representative Pb-soaked paper strips have a brown stain of PbS. **c** and (**d**) The accumulation of intracellular cysteine (μmol/10^9 cell, **c**) and cystine (μmol/10^9 cell, **d**) after co-cultured with PLP (ranging from 0 to 20 mM). **e** ROS production of *E. coli* G92 after incubation with PLP (ranging from 0 to 20 mM), determined using DCFH-DA (10 μM). **f** Percent survival of *E. coli* G92 co-incubated with PLP (10 mM) and colistin (2 μg/mL) for 4 or 8 h in the presence or absence of thiourea (10 mM). **g** The level of superoxide dismutase (SOD) activity of *E. coli* G92 during incubation with PLP (ranging from 0 to 20 mM). All data from three biological replicates were presented as mean ± SD, and statistical significance was determined by non-parametric one-way ANOVA. *$P < 0.05$, **$P < 0.01$, ***$P < 0.001$, ****$P < 0.0001$.

intraperitoneally with a lethal dose of *E. coli* G92 and sequentially treated with colistin with or without PLP. In the experimental group, a single colistin co-treatment with PLP significantly increased the 5-day survival rate of mice ($P = 0.0041$, Fig. 6d) and decreased the bacterial loads in the liver and kidney (Fig. 6e). Next, we measured cytokine levels in the liver using ELISA. Notably, we found that four proinflammatory cytokines, including TNF-α, IFN-γ, IL-1β and IL-6, were significantly decreased in the combination group, and anti-inflammatory factor IL-4 was increased (Fig. 6f), demonstrating that PLP alleviated inflammatory responses in mice. Meanwhile, we performed hematoxylin and eosin (H&E) staining to evaluate the liver and kidney damage. In both the liver and kidney, the pathological lesions, such as inflammatory cell infiltration, were most serious in the PBS group. Colistin treatment alleviated some of these lesions, while combined treatment with colistin and PLP eliminated the lesions altogether (Fig. 6g). These results indicate that PLP improves the therapeutic effect of colistin in multiple animal models of infection.
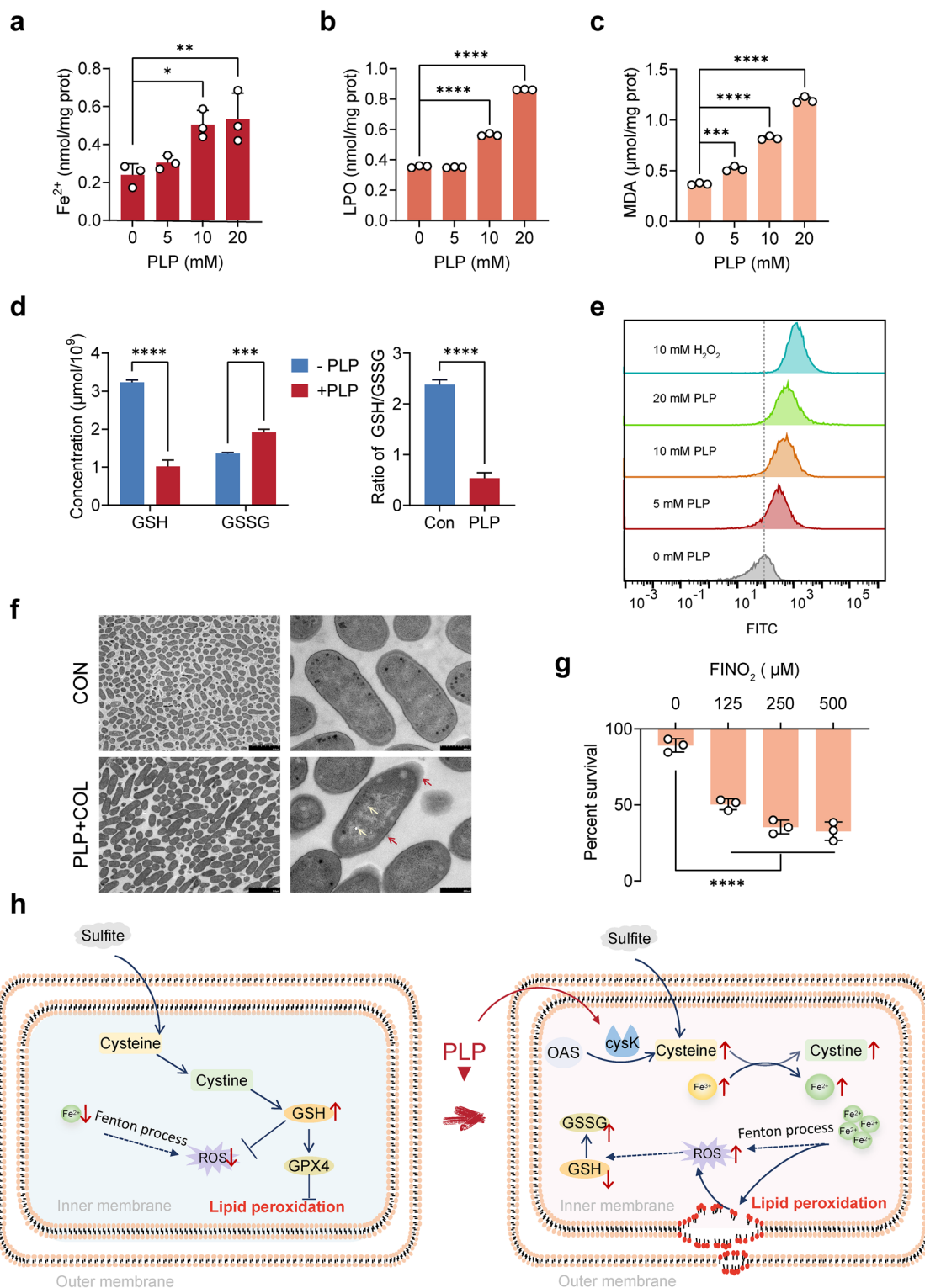
Fig. 5 | PLP triggers ferroptosis-like death in *mcr*-carrying bacteria. a The collection of Fe^{2+} (nmol/mg prot) in *E. coli* G92 after being treated by PLP (ranging from 0 to 20 mM). **b** and (**c**) LPO (**b**) and MDA (**c**) analysis of *E. coli* G92 in the presence of increasing concentrations of PLP (ranging from 0 to 20 mM). **d** Intracellular GSH and GSSG levels and the ratio of GSH/GSSG of *E. coli* G92 after co-culturing with PLP (10 mM). **e** The level of lipid peroxidation in *E. coli* G92 treated with different concentrations of PLP (ranging from 0 to 20 mM). H_2O_2-treated bacteria were used as positive control. **f** TEM images of *E. coli* G92 cells treated with PBS or PLP (10 mM) along with colistin (1 μg/mL). Scale bar, 5 μm (left) or 500 nm (right). **g** Percent survival of *E. coli* G92 in the presence of ferroptosis agonist $FINO_2$ (ranging from 0 to 500 μM) plus colistin (4 μg/mL). **h** Schematic illustration of modes of action of PLP in inducing ferroptosis-like death. All data from three biological replicates were presented as mean ± SD, and statistical significance was determined by non-parametric one-way ANOVA. *$P < 0.05$, **$P < 0.01$, ***$P < 0.001$, ****$P < 0.0001$.
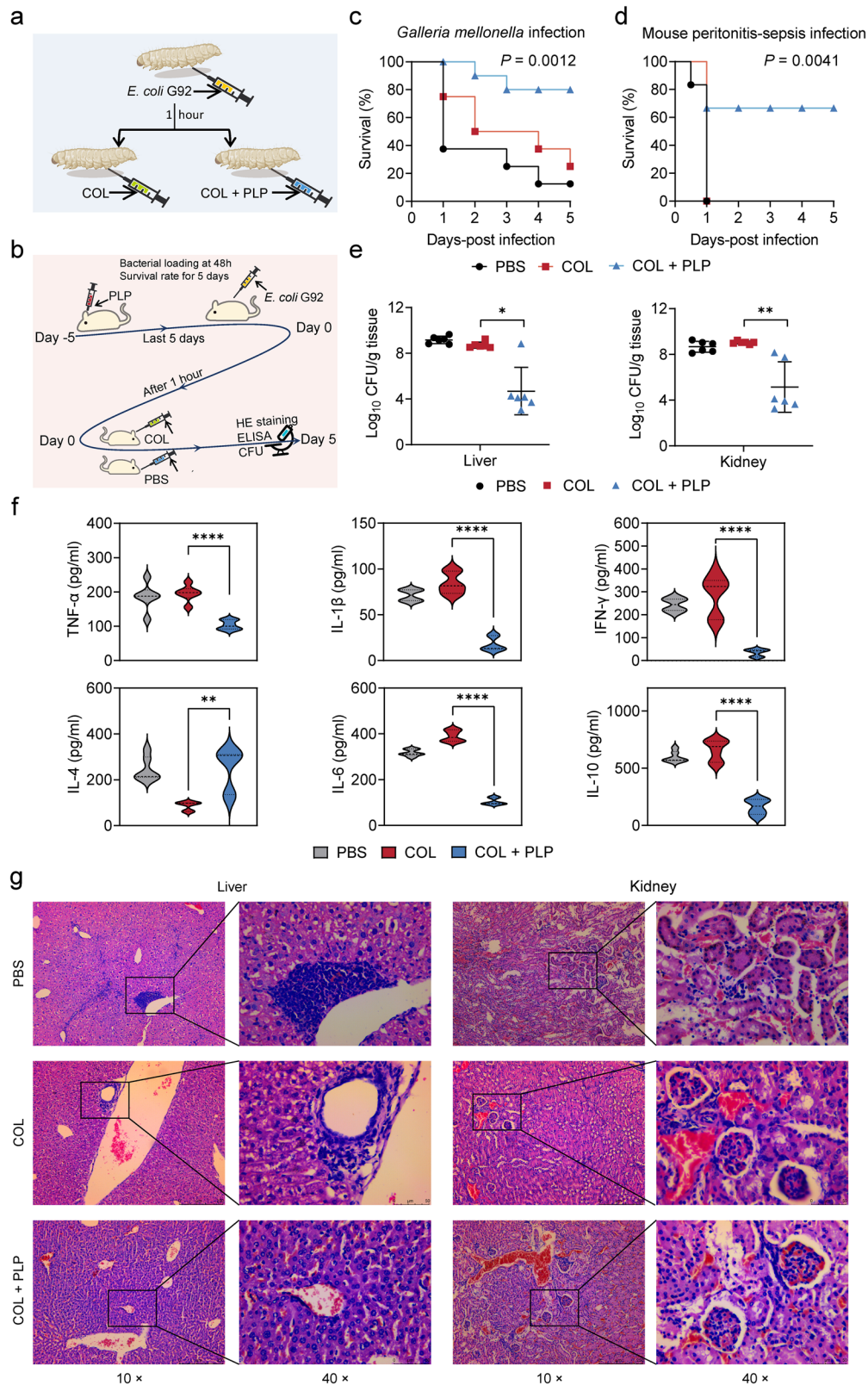
Discussion

Antimicrobial resistance (AMR) represents a global health crisis, contributing to elevated morbidity and mortality rates[52,53]. Colistin is one of the few effective medications against MDR Gram-negative infections. However, its efficacy is compromised by the widespread dissemination of the plasmid-mediated colistin resistance gene *mcr*[4]. Novel therapeutic choices and antimicrobial alternatives to antibiotics are urgently required. It has been posited that bacterial metabolic status is associated with the effectiveness of antibiotic therapy[34]. Drug-resistant bacteria, whether induced in the laboratory or isolated clinically, had altered metabolism compared with the original susceptible bacteria[34,54,55]. Thus, reshaping the metabolism of resistant bacteria represents a distinct strategy to tackle antibiotic resistance.

Fig. 6 | PLP administration enhances colistin effectiveness *in vivo*. a Scheme of the experimental protocols for *G. mellonella* larvae infection. **b** Scheme of the experimental protocols for mouse peritonitis-sepsis infection. **c** Survival rates of the *G. mellonella* larvae (n = 8 biologically independent animals per group) infected by *E. coli* G92 (2.0×10^6 CFUs), and then treated with a single dose of colistin (5 mg/kg) plus PLP (0.25 mg/kg). *P* values were determined by log-rank (Mantel-Cox) test. **d** Survival rates of the female BALB/c mice (n = 6 biologically independent animals per group) infected intraperitoneally by a lethal dose of *E. coli* G92 (5.0×10^8 CFUs) and then treated with PBS or colistin (2 mg/kg). Mice were pre-administered with PBS or PLP (10 mg/kg) for 5 consecutive days. *P* values were determined by log-rank

(Mantel–Cox) test. **e** Bacterial loads in mice liver and kidney. BALB/c mice (n = 6 biologically independent animals per group) were pre-administrated with PBS or PLP (10 mg/kg) for 5 consecutive days. Then they were intramuscularly given a non-lethal dose of *E. coli* G92 (1.0×10^6 CFUs), and treated with a single dose of either colistin (2 mg/kg) or PBS. Data were expressed as mean ± SD. *P* values were determined by Mann–Whitney *U*-test. *$P < 0.05$, **$P < 0.01$. **f** ELISA analysis of inflammatory cytokines in liver tissues of mice. Data were presented as mean ± SD. *P* values were determined by Student's *t*-test. **$P < 0.01$, ****$P < 0.0001$. **g** H&E staining of mice liver and kidney under different treatments.

In this study, we revealed that the presence of *mcr-1* gene altered the metabolic characteristics and metabolic flux of the host bacteria. Notably, the replenishment of PLP, the active form of vitamin B6, which was significantly depleted in *mcr-1*-positive bacteria, resensitized drug-resistant bacteria to colistin therapy. Unlike other drug combination strategies, such as the use of melatonin[56], saturated fatty acids[57] and SLAP-S25[58] as colistin synergists, or combinations of other antibiotics[59,60], which may introduce new resistance determinants, PLP-based metabolic reprogramming approach is safe and unlikely to result in drug resistance.

MCR protein can add phosphoethanolamine to lipid A, thereby reducing the electrostatic interaction between colistin and LPS[61]. Our results indicated that PLP augmented bacterial PMF, which is critical to the bactericidal action of colistin. In agreement with our findings, prior research has shown that boosting PMF can strengthen the binding of colistin to lipid A in LPS[34]. Furthermore, we found that the elevated PMF results from the repression of the Kdp system in bacteria exposed to PLP. The Kdp system is an ATP-dependent transmembrane transport system[62], and its inactivation leads to hyperpolarization of the membrane[32], which in turn stimulates ATP production and activates bacterial metabolism. This also suggests that the Kdp system may represent a novel target for novel antimicrobial agents.

Additionally, we found that siderophore-related genes in *mcr*-positive bacteria were up-regulated in the presence of PLP. By contrast, a previous study has shown that the expression of bacterial iron storage-related genes was downregulated under polymyxin stress in *mcr-1*-harboring *E. coli*[54]. Combined with the apparent enhancement of sulfur metabolism, we found that PLP, acting as a coenzyme, significantly enhanced the activity of *cysk*-encoded O-acetylserine sulfhydrylase, which resulted in the accumulation of cysteine. Interestingly, cysteine has previously been shown to enhance the activity of bactericidal antibiotics against persistent Gram-negative bacteria[63]. It has also been discovered that cysteine can prevent antibiotic tolerance and resistance in *Mycobacterium tuberculosis* by enhancing bacterial respiration[44]. We discovered that when cysteine was transformed into cystine, ferric ions were also turned into ferrous ions, which led to the accumulation of ferrous ions. Further mechanistic research revealed that high ferrous ions caused ferroptosis-like death, resulting in lipid peroxidation damage, which vastly improves the bactericidal action of antibiotics[43,64]. The synergistic effect of ferroptosis agonists on colistin further solidifies the potential to overcome colistin resistance through ferroptosis-like mechanisms. In this study, we employed the term "ferroptosis-like" to emphasize the similarities between the phenomena observed in bacteria and the hallmark features of ferroptosis in eukaryotic cells, such as lipid peroxidation and iron dependency. This terminology, however, does not imply that bacteria undergo a form of programmed cell death analogous to the regulated ferroptosis pathways observed in eukaryotes. In contrast to eukaryotic ferroptosis, which is governed by specific genetic and signaling cascades, the bacterial ferroptosis-like death described here is triggered by metabolic disruptions.

Another intriguing observation was that PLP possesses the capacity to mitigate the inflammatory response elicited by bacteria and concomitantly reduce kidney impairment in mice. This phenomenon may be associated with vitamin B6, of which PLP is the active metabolite. Vitamin B6, an excellent antioxidant, can be utilized not only simply as a nutritional supplement but also as a pharmacological agent in the treatment of various

disorders[65]. Notably, vitamin B6 has been shown to modulate IL-33 homeostasis, effectively alleviating type 2 inflammation[66], and its supplementation has demonstrated efficacy in ameliorating inflammatory bowel disease (IBD) in mice[28]. Nevertheless, the potential of PLP to counteract the nephrotoxicity and neurotoxicity induced by colistin merits further investigation.

Although vitamin B6 is abundant in the human diet, its clinical efficacy in patients infected with colistin-resistant strains may be compromised by chromosomal mutations. These mutations are more challenging to counter with dietary interventions or supplementation alone. In clinical contexts, bacterial populations frequently harbor multiple genetic resistance mechanisms, including efflux pumps and LPS modifications, which can diminish the efficacy of monotherapies like PLP. Therefore, more investigations are required to evaluate the therapeutic potential of PLP against other determinants of colistin resistance, such as mutations in the PhoPQ system or lipid A modification genes.

In summary, our study presents a pioneering metabolic reprogramming-based strategy to resensitize MDR Gram-negative bacteria to colistin treatment. Specifically, we demonstrate that the supplementation of PLP can effectively counteract *mcr*-mediated colistin resistance by inhibiting the Kdp transport system and triggering ferroptosis-like death, thereby enhancing the therapeutic efficacy of this last-resort antibiotic. These findings open new avenues for curbing the rise of AMR in clinical settings.

Methods
Antibiotics and chemicals
All antibiotics were sourced from the China Institute of Veterinary Drug Control. Antibiotics were dissolved in water, filtered through a 0.22 μm pore size membrane. The drug was available as hydrochloride or sulfate, all doses were calculated as salts. Other chemical reagents were obtained from Aladdin (Shanghai, China) or Sigma-Aldrich (Oakville, Ontario). Pyridoxal 5'-phosphate (PLP) was dissolved in 1 M NaOH. To ensure that reagents were preserved, they were stored at $-20\,°C$.

Strains and culture methods
All the bacterial strains (documented in Table S5) were stored in aliquots (containing 20% glycerol) at $-80\,°C$ before use. The bacteria were revived on Luria-Bertani agar (LBA) and cultured in Mueller-Hinton broth (MHB) at 37 °C for 16 h with shaking at 200 rpm for further use. PLP and antibiotic MICs were calculated based on two-fold serial dilutions in MHB before incubation at 37 °C for 18 h.

Effect of metabolites on antibiotic killing
Bacteria were diluted 1:100 in 10 mL of fresh MHB medium for 4 h at 37 °C with shaking at 200 rpm. Before being resuspended in M9CA medium (Sangon Biotech, Shanghai, China) for another 4 h, they were collected, washed three times with phosphate-buffered saline (PBS). The blank control group did not contain antibiotics, while the experimental group contained different antibiotics (2-fold MIC) with or without metabolites (10 mM). The bacterial solution of 50 μL was taken after serial dilution, spot-plated on LB plates, and colony-forming units (CFUs) were counted.

Untargeted metabolomics analysis

E. coli DH5α (pUC19) and *E. coli* DH5α (pUC19-*mcr-1*) cultures were diluted 1:100 into 10 mL of fresh MHB and cultivated for 4 h. For metabolite extraction, 300 μL of methanol:acetonitrile (2:1, v/v) was added to 100 μL of sample, with L-2-chlorophenylalanine used as an internal standard. The mixture was vortexed for 30 seconds, sonicated at low temperature for 15 min, and then placed at −20 °C for 30 min. After centrifugation at 13,000 rpm for 15 min at 4 °C, the supernatant was dried under nitrogen.

Next, 80 μL of methoxypyridine hydrochloride (15 mg/mL) was added, and the sample was vortexed and incubated at 37 °C for 90 min for oximation. The sample was then supplemented with 80 μL of BSTFA containing 1% TMCS, vortexed for 2 min, and incubated at 70 °C for 60 min for derivatization. The prepared samples were analyzed by GC–MS using an Agilent 8890B gas chromatograph coupled with an Agilent 5977B mass selective detector.

A quality control (QC) sample was included to ensure system reliability. Raw data were processed using MassHunter Workstation Quantitative Analysis software (v10.0.707.0).

Transcriptomic analysis

E. coli DH5α (pUC19) and *E. coli* DH5α (pUC19-*mcr-1*) were diluted 1:100 into 10 mL of fresh MHB and cultured for 4 h. For *E. coli* G92 (*mcr-1*), cultures were diluted 1:100 into 10 mL of fresh MHB supplemented with or without PLP (1 mM) and incubated for 4 h under identical conditions. After incubation, bacterial cells were harvested and washed three times with PBS. Transcriptomic analysis was performed using the TruSeq™ Stranded Total RNA Library Prep Kit to construct sequencing libraries, following a previously established method[67]. Sequencing was conducted on the Illumina HiSeq platform, generating paired-end reads of 2×150 bp. Gene annotation was performed by comparing the sequences with the KEGG and GO databases. Quantitative analysis of transcript expression levels was conducted using RSEM. The newly generated transcriptomic data from the PLP-treated samples were deposited in the NCBI database under the existing BioProject (accession number: PRJNA1011224). This dataset includes both the previously published transcriptomic data of *E. coli* G92 treated with potassium sorbate (PS)[6] and the data generated in this study for PLP treatment.

Live/dead BacLight viability assay

Overnight cultures of *E. coli* DH5α (pUC19-*mcr-1*), *E. coli* G92 (*mcr-1*), *Salmonella enterica* SC2016090 (*mcr-3*), and *Klebsiella pneumoniae* D120 (*mcr-8*) were diluted in MHB for 4 h, then transferred to M9CA medium and co-cultured with colistin ($2 \times$ MIC) and PLP (10 mM) individually or in combination. SYTO 9 (2.5 μM) and propidium iodide (PI, 5 μM) were added and incubated in the dark at room temperature for 30 min. Flow cytometry (CytExpert, Beckman) was used to measure 100,000 events, with forward scatter (FSC) and side scatter (SSC) to exclude debris and FSC-A/FSC-H gating to remove doublets. Confocal microscopy (Leica TCS SP8) was used to visualize live (green) and dead (red) bacteria.

Bacterial growth curve

E. coli G92 diluted 1:1000 with MHB broth after overnight culture. The absorbance of the bacterial solution at 600 nm was adjusted to 0.1, and then bacteria were incubated with colistin (1/2-fold MIC) compared with or without PLP (10 mM). The culture was then shaken at 200 rpm at 37 °C for 12 h. During this period, the absorbance of the bacterial solution at 600 nm was detected every 0.5 h.

Biochemical factors analysis

E. coli G92 in the logarithmic growth phase was resuspended in M9CA medium. Fluorescent probes were added and incubated at 37 °C for 30–60 min. The probe-labeled bacteria were then transferred to a 96-well plate containing different concentrations of PLP (0, 5, 10, and 20 mM). After incubation for 1 h at 37 °C in the dark, fluorescence intensity was measured using a microplate reader (Infinite E Plex).

Cell membrane integrity. A fluorescent probe propidium iodide[35] (PI, 5 μM) was used. The fluorescence intensity was measured at the excitation/emission wavelength of 535/615 nm.

Potassium efflux. Potassium-binding benzofuran lsophthalate acetoxymethyl[68] (PBFI AM, 5 μM) in the presence of 0.05% (w/w) Pluronic F-127 was used to detect the activity of potassium efflux. The fluorescence intensity was measured at the excitation/emission wavelength of 340/500 and 380/500 nm.

Membrane depolarization. 3,3'-Dipropyl-thiacarbocyanine iodide[10] (DiSC$_3$(5), 0.5 μM) was used to measure membrane potential change. The fluorescence intensity was measured at the excitation/emission wavelength of 622/670 nm.

Outer membrane permeability. *N*-phenyl-1-naphthylamine[56] (NPN, 10 μM) was used to measure outer membrane permeability. The fluorescence intensity was measured at the excitation/emission wavelength of 350/420 nm.

Intracellular pH. 2',7'-bis-(2-carboxyethyl)-5-(and-6)-carboxyfluorescein acetoxymethy[69] (BCECF AM, 1 μM) was used to analyze intracellular pH. The fluorescence intensity was measured at the excitation/emission wavelength of 488/535 nm.

Total ROS production

ROS production in *E. coli* G92 was analyzed using 2',7'-Dichlorodihydrofluorescein diacetate[70] (DCFH-DA, 10 μM). After labeling, the bacteria were then washed and resuspended by M9CA, and co-cultured with PLP (0, 5, 10, 20 mM). Thiourea (10 mM) was used as a ROS scavenger. The fluorescence intensity was measured at the excitation/emission wavelength of 488/525 nm.

Total ATP levels

E. coli G92 was diluted 1:100 into 10 mL of fresh medium and cultured for 4 h. The cells were then resuspended in M9CA medium and co-cultured with PLP (0, 5, 10, 20 mM) for an additional 4 h. The ATP levels in *E. coli* G92 were quantified using the Enhanced ATP Assay Kit (Beyotime, China) according to the manufacturer's instructions. The content was normalized to the total protein content and expressed as units/g protein. Relative luminescence units (RLU) were measured using the Infinite E Plex system (Tecan) and the ATP concentration was determined based on standard curves.

NAD$^+$/NADH, ferrous iron, lipid peroxide (LPO) and malondialdehyde contents (MDA)

Bacterial cultures were prepared as described previously. The NAD$^+$/NADH levels in *E. coli* G92 treated with PLP were measured using the NAD$^+$/NADH Assay Kit with WST-8 (Beyotime). Initially, the total NAD content was quantified. To specifically detect NADH, samples were heated at 60 °C for 30 min to decompose NAD$^+$. The NAD$^+$ content was then calculated by subtracting the NADH content from the total NAD.

The Fe^{2+} content was measured using Ferrous Ion Content Assay Kit (Solarbio). The intracellular LPO content was determined using Lipid Peroxide (LPO) Content Assay Kit (Solarbio). The intracellular MDA content was monitored using Malondialdehyde (MDA) Content Assay Kit (Beyotime).

Glutathione (GSH), glutathione oxidized (GSSG), superoxide dismutase (SOD) activity

The GSH and GSSG contents were measured using the GSH and GSSG Assay Kit (Beyotime). The total GSH concentration was determined at 412 nm. GSH levels were calculated by subtracting GSSG from the total glutathione. Specifically, GSSG was first isolated from the sample using a

https://doi.org/10.1038/s42003-025-07911-5

Article

GSH removal auxiliary solution, then reduced to GSH by glutathione reductase, and its concentration was measured at 410 nm.

SOD activity was assessed using the Total Superoxide Dismutase Assay Kit with WST-8 (Beyotime) in *E. coli* G92 treated with PLP (0–20 mM).

Bacterial proton motive force (PMF) analysis

E. coli G92 was cultured overnight and resuspended (1:100 dilution) in fresh MH for 4 h. Dye-free samples were used to control for autofluorescence. PMF was determined by 3, 3'-diethyloxa-carbocyanine iodide[71] (DiOC$_2$(3), 60 μM). *E. coli* G92 was processed as described previously and co-incubated with DiOC$_2$(3) at 37 °C for 15 min. Carbonyl cyanide 3-chlorophenylhydrazone (CCCP, 5 μM) was used as the depolarized control sample. Green fluorescence was detected using a 488–530 nm bandpass filter, and red fluorescence was detected using a 488–610 nm bandpass filter. A CytExpert Flow Cytometer recorded 100,000 ungated events per sample, which were analyzed using FlowJo 10.8.1 software (Becton, Dickinson and Company, USA). Debris was excluded based on forward scatter (FSC) and side scatter, and single bacterial cells were gated using FSC-A vs. FSC-H. Unstained bacteria served as blank controls for autofluorescence, and CCCP-treated cells were used as negative controls to establish a low PMF threshold.

Lipid peroxidation assay

Lipid peroxidation was assessed using C11-BODIPY (10 μM). *E. coli* G92 was incubated with C11-BODIPY and PLP (0, 5, 10, 20 mM) at 37 °C for 90 min. H$_2$O$_2$ (10 μM) was used as a positive control for lipid peroxidation. Green fluorescence was detected using a 488–530 nm bandpass filter. Each sample was analyzed using a CytExpert Flow Cytometer, recording 100,000 ungated events, and data were processed with FlowJo 10.8.1 software. Lipid peroxidation was evaluated by comparing green (non-peroxidized) and red (peroxidized) fluorescence channels. An unstained control was used to set the baseline for autofluorescence, while H$_2$O$_2$-treated cells served as a positive control for peroxidation.

H$_2$S production

H$_2$S production in *E. coli* G92 was monitored using the lead acetate detection method. *E. coli* G92 was diluted 1:100 and incubated with PLP (0, 5, 10, 20 mM) and colistin (1 μg/mL) at 37 °C for 15 h. A paper strip saturated with 2% lead acetate (Pb(Ac)$_2$) was placed above the liquid culture, affixed to the inner wall of the culture tube. Darkening of the paper strip indicated H$_2$S generation, with darker color corresponding to higher H$_2$S production.

Transmission electron microscopy (TEM)

E. coli G92 was cultured overnight and then diluted 1:100 into MHB for 4 h. The cultures were subsequently incubated with PLP ranging from 0 to 20 mM for an additional 4 h. The bacteria were then fixed with 2.5% glutaraldehyde, followed by post-fixation in 1% osmium tetroxide. After fixation, the samples were dehydrated using a graded series of ethanol concentrations and embedded in epoxy resin.

Reverse transcription-quantitative PCR (RT-qPCR)

E. coli G92 was cultured until reaching the stationary phase and diluted at a ratio of 1:100 into MH for 4 h with or without PLP. Following this, the bacterial cells were washed with PBS three times. RNA extraction and purification and RT-qPCR were carried out as previously described. The total RNA was extracted by Bacteria RNA Extraction Kit (Vazyme, China) and reverse-transcribed using PrimeScript™ RT Kit and gDNA Eraser (Takara, China). RT-qPCR analysis was performed by 7500 Fast Real-Time PCR System (Applied Biosystem, CA, USA) using the ChamQ SYBR Color qPCR Master Mix (Vazyme) with the primers (Table S6). The thermal cycling procedure involved two steps of PCR amplification. Based on the $2^{-\Delta\Delta Ct}$ method, the fold change in mRNA expression was calculated relative to a reference gene (16S rRNA).

Single nucleotide polymorphisms (SNPs) analysis

Genomic DNA was extracted from bacterial samples using the Bacterial DNA Kit D3350 (Omega Bio-tek, USA), and its quality and quantity were assessed with a NanoDrop spectrophotometer. Library preparation was followed by sequencing on an Illumina NovaSeq 6000 platform. Raw data were quality-checked with FastQC and trimmed using Trim Galore. The genome was assembled and annotated using the RAST server. SNPs were identified by aligning the reads to a reference genome with BWA.

Galleria mellonella infection model

Galleria mellonella larvae (Huiyude Biotech Company, Tianjin, China) were randomly assigned to three groups ($n = 8$ each group). Then, they were infected with *E. coli* G92 suspension (10 μL, 1.0×10^6 CFUs). After one hour of infection, larvae were treated with PBS or colistin (40 mg/kg) with or without PLP. Survival rates of larvae were recorded for a period of five days.

Ethical statement

Animal experiments were conducted in compliance with the applicable guidelines and regulations set forth by Jiangsu Laboratory Animal Welfare and Ethical of Jiangsu Administrative Committee of Laboratory Animals (SCXK-2022-0044). The use of experimental animals was authorized by the Jiangsu Association for Science and Technology under license number SCXK-2022-0009. All animal experiments were approved by the Animal Care Committee of Yangzhou University, and we have complied with all relevant ethical regulations for animal use.

Mouse peritonitis-sepsis infection model

Female BALB/c mice (aged 6-8 weeks) were procured from the Comparative Medicine Centre of Yangzhou University (Jiangsu, China). Mice were acclimatized for one week before being infected. A total of 36 female BALB/c mice were intraperitoneally injected with PBS ($n = 24$) or 10 mg/kg PLP ($n = 12$) for five days, and then intraperitoneally infected with *E. coli* G92 suspension at a dose of 5.0×10^8 CFUs or 1.0×10^6 CFUs. After one hour of infection, the mice of PBS group were randomly divided into blank control group ($n = 12$) and antibiotic groups ($n = 12$). The blank control group received a single intraperitoneal dose of PBS, while the antibiotic treatment group and PLP group received colistin at a dosage of 2 mg/kg. The survival of the mice was monitored for a period of 5 days. The liver and kidney were aseptically removed and separated into two parts for CFUs estimation, HE staining and ELISA analysis.

Statistics and reproducibility

Statistical analyses were performed using GraphPad Prism version 9.0. Each experiment included at least three independent biological replicates. Data are presented as mean ± standard deviation (SD). For in vitro experiments, statistical significance was assessed using unpaired *t*-test or one-way ANOVA. For in vivo studies, significance was determined using the log-rank (Mantel–Cox) test or the Mann-Whitney *U*-test. Significance levels were defined as: $*P < 0.05$, $**P < 0.01$, $***P < 0.001$, and $****P < 0.0001$.

Data availability

RNA-sequencing data have been deposited in the National Center for Biotechnology Information (NCBI) Sequence Read Archive (SRA) database (PRJNA1011224). Source data for the main figures are provided in Supplementary Data 1. All other data are available from the corresponding authors.

References

1. Li, J. et al. Colistin: the re-emerging antibiotic for multidrug-resistant Gram-negative bacterial infections. *Lancet Infect. Dis.* **6**, 589–601 (2006).

2. Nang, S. C., Azad, M. A. K., Velkov, T., Zhou, Q. T. & Li, J. Rescuing the last-line polymyxins: achievements and challenges. *Pharmacol. Rev.* **73**, 679–728 (2021).

3. Taglialegna, A. Reviving colistin. *Nat. Rev. Microbiol.* **21**, 411 (2023).

4. Wang, R. et al. The global distribution and spread of the mobilized colistin resistance gene *mcr-1*. *Nat. Commun.* **9**, 1179 (2018).

5. Dalmasso, G. et al. Genes mcr improve the intestinal fitness of pathogenic *E. coli* and balance their lifestyle to commensalism. *Microbiome* **11**, 12 (2023).

6. Xu, T., Fang, D., Li, F., Wang, Z. & Liu, Y. A dietary source of high level of fluoroquinolone tolerance in *mcr*-carrying Gram-negative bacteria. *Research* **6**, 0245 (2023).

7. Stokes, J. M., Lopatkin, A. J., Lobritz, M. A. & Collins, J. J. Bacterial metabolism and antibiotic efficacy. *Cell Metab.* **30**, 251–259 (2019).

8. Zeng, J. et al. A broadly applicable, stress-mediated bacterial death pathway regulated by the phosphotransferase system (PTS) and the cAMP-Crp cascade. *Proc. Natl Acad. Sci. USA* **119**, e2118566119 (2022).

9. Liu, Y. et al. Gut microbiome alterations in high-fat-diet-fed mice are associated with antibiotic tolerance. *Nat. Microbiol.* **6**, 874–884 (2021).

10. Liu, Y. et al. Sodium dehydroacetate confers broad antibiotic tolerance by remodeling bacterial metabolism. *J. Hazard. Mater.* **432**, 128645 (2022).

11. Martínez, J. L. & Rojo, F. Metabolic regulation of antibiotic resistance. *FEMS Microbiol. Rev.* **35**, 768–789 (2011).

12. Helling, R. B. & Kukora, J. S. Nalidixic acid-resistant mutants of Escherichia coli deficient in isocitrate dehydrogenase. *J. Bacteriol.* **105**, 1224–1226 (1971).

13. Gruer, M. J., Bradbury, A. J. & Guest, J. R. Construction and properties of aconitase mutants of *Escherichia coli*. *Microbiology* **143**, 1837–1846 (1997).

14. Schurek, K. N. et al. Novel genetic determinants of low-level aminoglycoside resistance in *Pseudomonas aeruginosa*. *Antimicrob. Agents Chemother.* **52**, 4213–4219 (2008).

15. Choi, J. S., Seok, Y. J., Cho, Y. H. & Roe, J. H. Iron-induced respiration promotes antibiotic resistance in *Actinomycete* bacteria. *mBio* **13**, e0042522 (2022).

16. Yeom, J., Imlay, J. A. & Park, W. Iron homeostasis affects antibiotic-mediated cell death in *Pseudomonas* species. *J. Biol. Chem.* **285**, 22689–22695 (2010).

17. Lu, Y. et al. Overexpression of *mcr-1* disrupts cell envelope synthesis and causes the dysregulation of carbon metabolism, redox balance and nucleic acids. *Int. J. Antimicrob. Agents* **60**, 106643 (2022).

18. Liu, Y. et al. Thymine sensitizes Gram-negative pathogens to antibiotic killing. *Front. Microbiol.* **12**, 622798 (2021).

19. Zhao, X.-l. et al. Glutamine promotes antibiotic uptake to kill multidrug-resistant uropathogenic bacteria. *Sci. Transl. Med.* **13**, eabj0716 (2021).

20. Peng, B. et al. Exogenous alanine and/or glucose plus kanamycin kills antibiotic-resistant bacteria. *Cell Metab.* **21**, 249–262 (2015).

21. Hoegl, A. et al. Mining the cellular inventory of pyridoxal phosphate-dependent enzymes with functionalized cofactor mimics. *Nat. Chem.* **10**, 1234–1245 (2018).

22. Percudani, R. & Peracchi, A. A genomic overview of pyridoxal-phosphate-dependent enzymes. *EMBO Rep.* **4**, 850–854 (2003).

23. Tynes, M., Hepprich, M. & Timper, K. Regular intake of energy drinks and multivitamin supplements is associated with elevated plasma vitamin B6 levels in post-bariatric patients. *Sci. Rep.* **11**, 17830 (2021).

24. John, R. A. Pyridoxal phosphate-dependent enzymes. *Biochim. Biophys. Acta* **1248**, 81–96 (1995).

25. Cheng, C.-H. et al. Plasma pyridoxal 5'-phosphate and high-sensitivity C-reactive protein are independently associated with an increased risk of coronary artery disease. *Nutrition* **24**, 239–244 (2008).

26. Hron, G. et al. Low vitamin B6 levels and the risk of recurrent venous thromboembolism. *Haematologica* **92**, 1250–1253 (2007).

27. Friedman, A. N., Hunsicker, L. G., Selhub, J. & Bostom, A. G. Clinical and nutritional correlates of C-reactive protein in type 2 diabetic nephropathy. *Atherosclerosis* **172**, 121–125 (2004).

28. Selhub, J. et al. Dietary vitamin B6 intake modulates colonic inflammation in the IL10$^{-/-}$ model of inflammatory bowel disease. *J. Nutr. Biochem.* **24**, 2138–2143 (2013).

29. Pfanzelt, M., Maher, T. E., Absmeier, R. M., Schwarz, M. & Sieber, S. A. Tailored pyridoxal probes unravel novel cofactor-dependent targets and antibiotic hits in critical bacterial pathogens. *Angew. Chem. Int. Ed. Engl.* **61**, e202117724 (2022).

30. Janssen, A. B., van Hout, D., Bonten, M. J. M., Willems, R. J. L. & van Schaik, W. Microevolution of acquired colistin resistance in Enterobacteriaceae from ICU patients receiving selective decontamination of the digestive tract. *J. Antimicrob. Chemother.* **75**, 3135–3143 (2020).

31. Silberberg, J. M. et al. Deciphering ion transport and ATPase coupling in the intersubunit tunnel of KdpFABC. *Nat. Commun.* **12**, 5098 (2021).

32. Liu, X. et al. The potassium transporter KdpA affects persister formation by regulating ATP levels in *Mycobacterium marinum*. *Emerg. Microbes Infect.* **9**, 129–139 (2020).

33. Epstein, W., Whitelaw, V. & Hesse, J. A. K. transport ATPase in *Escherichia coli*. *J. Biol. Chem.* **253**, 6666–6668 (1978).

34. Li, L., Su, Y. B., Peng, B., Peng, X. X. & Li, H. Metabolic mechanism of colistin resistance and its reverting in *Vibrio alginolyticus*. *Environ. Microbiol.* **22**, 4295–4313 (2020).

35. Sabnis, A. et al. Colistin kills bacteria by targeting lipopolysaccharide in the cytoplasmic membrane. *Elife* **10**, e65836 (2021).

36. Silhavy, T. J. & Beckwith, J. Isolation and characterization of mutants of *Escherichia coli* K12 affected in protein localization. *Methods Enzymol.* **97**, 11–40 (1983).

37. Fravega, J. et al. *Salmonella* Typhimurium exhibits fluoroquinolone resistance mediated by the accumulation of the antioxidant molecule H2S in a CysK-dependent manner. *J. Antimicrob. Chemother.* **71**, 3409–3415 (2016).

38. Lacourciere, G. M., Levine, R. L. & Stadtman, T. C. Direct detection of potential selenium delivery proteins by using an Escherichia coli strain unable to incorporate selenium from selenite into proteins. *Proc. Natl Acad. Sci. USA* **99**, 9150–9153 (2002).

39. Zhou, Y. & Imlay, J. A. *Escherichia coli* K-12 lacks a high-affinity assimilatory cysteine importer. *mBio* **11**, e01073–20 (2020).

40. Shatalin, K., Shatalina, E., Mironov, A. & Nudler, E. H2S: a universal defense against antibiotics in bacteria. *Science* **334**, 986–990 (2011).

41. Kohanski, M. A., DePristo, M. A. & Collins, J. J. Sublethal antibiotic treatment leads to multidrug resistance via radical-induced mutagenesis. *Mol. Cell* **37**, 311–320 (2010).

42. Olson, K. R. et al. Metabolism of hydrogen sulfide (H2S) and production of reactive sulfur species (RSS) by superoxide dismutase. *Redox Biol.* **15**, 74–85 (2018).

43. Kohanski, M. A., Dwyer, D. J., Hayete, B., Lawrence, C. A. & Collins, J. J. A common mechanism of cellular death induced by bactericidal antibiotics. *Cell* **130**, 797–810 (2007).

44. Vilcheze, C. et al. Enhanced respiration prevents drug tolerance and drug resistance in *Mycobacterium tuberculosis*. *Proc. Natl Acad. Sci. USA* **114**, 4495–4500 (2017).

45. Zhong, Z.-X. et al. Natural flavonoids disrupt bacterial iron homeostasis to potentiate colistin efficacy. *Sci. Adv.* **9**, eadg4205 (2023).

46. Hadian, K. & Stockwell, B. R. SnapShot: ferroptosis. *Cell* **181**, 1188–1188.e1 (2020).

47. Muckenthaler, M. U., Rivella, S., Hentze, M. W. & Galy, B. A red carpet for iron metabolism. *Cell* **168**, 344–361 (2017).

48. Yang, W. S. et al. Peroxidation of polyunsaturated fatty acids by lipoxygenases drives ferroptosis. *Proc. Natl Acad. Sci. USA* **113**, E4966–E4975 (2016).

49. Sun, B. et al. Designing single-atom active sites on sp2 -carbon linked covalent organic frameworks to induce bacterial ferroptosis-like for robust anti-infection therapy. *Adv. Sci.* **10**, e2207507 (2023).

50. Ma, R. et al. Ferroptotic stress promotes macrophages against intracellular bacteria. *Theranostics* **12**, 2266–2289 (2022).

51. Gaschler, M. M. et al. FINO2 initiates ferroptosis through GPX4 inactivation and iron oxidation. *Nat. Chem. Biol.* **14**, 507–515 (2018).

52. Frieri, M., Kumar, K. & Boutin, A. Antibiotic resistance. *J. Infect. Public Health* **10**, 369–378 (2017).

53. Akova, M. Epidemiology of antimicrobial resistance in bloodstream infections. *Virulence* **7**, 252–266 (2016).

54. Nang, S. C. et al. Polymyxin causes cell envelope remodelling and stress responses in *mcr-1*-harbouring *Escherichia coli*. *Int. J. Antimicrob. Agents* **59**, 106505 (2022).

55. Li, H. et al. Comprehensive proteomic and metabolomic profiling of mcr-1-mediated colistin resistance in *Escherichia coli*. *Int. J. Antimicrob. Agents* **53**, 795–804 (2019).

56. Liu, Y. et al. Melatonin overcomes MCR-mediated colistin resistance in Gram-negative pathogens. *Theranostics* **10**, 10697–10711 (2020).

57. Cai, J. et al. Structural-activity relationship-inspired the discovery of saturated fatty acids as novel colistin enhancers. *Adv. Sci.* **10**, e2302182 (2023).

58. Song, M. et al. A broad-spectrum antibiotic adjuvant reverses multidrug-resistant Gram-negative pathogens. *Nat. Microbiol.* **5**, 1040–1050 (2020).

59. Motaouakkil, S. et al. Colistin and rifampicin in the treatment of nosocomial infections from multiresistant *Acinetobacter baumannii*. *J. Infect.* **53**, 274–278 (2006).

60. Scudeller, L. et al. Systematic review and meta-analysis of in vitro efficacy of antibiotic combination therapy against carbapenem-resistant Gram-negative bacilli. *Int. J. Antimicrob. Agents* **57**, 106344 (2021).

61. Son, S. J., Huang, R., Squire, C. J. & Leung, I. K. H. MCR-1: a promising target for structure-based design of inhibitors to tackle polymyxin resistance. *Drug Discov. Today* **24**, 206–216 (2019).

62. Epstein, W. et al. The bacterial Kdp K(+)-ATPase and its relation to other transport ATPases, such as the Na+/K(+)- and Ca2(+)-ATPases in higher organisms. *Philos. Trans. R. Soc. Lond. B Biol. Sci.* **326**, 479–486 (1990).

63. Liu, Y. et al. Cysteine potentiates bactericidal antibiotics activity against Gram-negative bacterial persisters. *Infect. Drug Resist.* **13**, 2593–2599 (2020).

64. Van Acker, H. & Coenye, T. The role of reactive oxygen species in antibiotic-mediated killing of bacteria. *Trends Microbiol.* **25**, 456–466 (2017).

65. Hellmann, H. & Mooney, S. Vitamin B6: a molecule for human health? *Molecules* **15**, 442–459 (2010).

66. Zhu, S. et al. Vitamin B6 regulates IL-33 homeostasis to alleviate type 2 inflammation. *Cell. Mol. Immunol.* **20**, 794–807 (2023).

67. Liu, Y. et al. Metformin restores tetracyclines susceptibility against multidrug resistant bacteria. *Adv. Sci.* **7**, 1902227 (2020).

68. Grieshaber, S., Swanson, J. A. & Hackstadt, T. Determination of the physical environment within the *Chlamydia trachomatis* inclusion using ion-selective ratiometric probes. *Cell. Microbiol.* **4**, 273–283 (2002).

69. Jiang, J. et al. Alkaline pH shock enhanced production of validamycin A in fermentation of *Streptomyces hygroscopicus*. *Bioresour. Technol.* **249**, 234–240 (2018).

70. Cui, Y. et al. The molecular mechanism of action of bactericidal gold nanoparticles on *Escherichia coli*. *Biomaterials* **33**, 2327–2333 (2012).

71. Su, Y.-B. et al. Pyruvate cycle increases aminoglycoside efficacy and provides respiratory energy in bacteria. *Proc. Natl Acad. Sci. USA* **115**, E1578–E1587 (2018).

Acknowledgements

Author contributions

Y.L. and Z.W. designed and supervised the project. T.X., D.F., and F.L. performed all experiments. Y.L. and T.X. analyzed the data and prepared all figures. Y.L. and T.X. wrote the manuscript. All the authors read and approved the final manuscript.

Competing interests

The authors declare no competing interests.

Additional information

Correspondence and requests for materials should be addressed to Zhiqiang Wang or Yuan Liu.

Peer review information *Communications Biology* thanks Juan Carlos Jimenez-Castellanos, Sun Ju Kim, and the other, anonymous, reviewer for their contribution to the peer review of this work. Primary Handling Editors: Haichun Gao and Michele Repetto.